

# Variation and Stochasticity in Polycrystalline HZO based MFIM: Grain-Growth Coupled 3D Phase Field Model based Analysis

R. Koduru, A. K. Saha, M. Si, X. Lyu, P. D. Ye, and S. K. Gupta  
Purdue University, West Lafayette, IN 47907, USA, email: [kodurur@purdue.edu](mailto:kodurur@purdue.edu)

**Abstract**— We present the first 3D phase-field simulation framework for ferroelectric (FE)  $\text{Hf}_{1-x}\text{Zr}_x\text{O}_2$  (HZO) based MFIM stack that self-consistently couples grain-growth, multi-domain (MD) polarization ( $P$ ) switching and electrostatics. Based on 3D grain-growth models, time-dependent Ginzburg-Landau (TDGL) equations and Poisson's equations, our framework captures the effects of polycrystalline grain size/shape distribution and inter- and intra-grain domain interactions. Using our model, we first analyze the implication of multi-domain  $P$ -switching in a single grain signifying the correlation of different macroscopic properties with respect to the crystal angle. Then we analyze, how the  $P$ -switching in one grain affects the  $P$ -switching in the neighboring grains. Next, we focus on the  $P$ -switching in a multi-grain scenario and analyze the sample-to-sample variations and cycle-to-cycle stochasticity in a small area FE sample. Finally, we show how FE thickness scaling (from 7nm to 3nm) can reduce variation and stochasticity in an MFIM stack by approximately 30%.

## I. INTRODUCTION

By virtue of its CMOS process compatibility, Hafnium Zirconium Oxide (HZO) based Ferroelectric (FE) devices are amongst the most promising candidates for future electronics. FE field-effect-transistors (FEFETs) and FE-tunnel-junctions (FTJs) have been demonstrated to offer multi-level memory and synaptic functionalities featuring stochasticity [1-2] and thus identified as potential candidates for neuromimetic hardware. While such functionalities are well demonstrated for large-area devices, the attainability of such functionalities were envisioned to be affected in small area devices due to polycrystallinity induced variation in the FE [3-5]. Most importantly, such forecasts are based on the nucleation limited switching (NLS) [4] and/or kinetic Monte-Carlo simulation with an assumption of single-domain (SD) switching in each grain with a coercive voltage distribution [5] (Fig. 1). At the same time, the possible origin of stochasticity and its controllability with respect to device optimization are yet to be explored.

To that end, in this work, we analyze multi-domain polarization ( $P$ ) switching in metal-ferroelectric-insulator-metal (MFIM) considering the multi-grain nature of polycrystalline HZO and provide insights into the effects of grain size/shape variation on the  $P$ -switching characteristics. For our analysis, we advance the current modeling approaches by building a fully self-consistent 3D phase-field simulation coupled with 3D grain growth models. We show that the intra-grain MD  $P$ -switching leads to a suppressed variation in FE characteristics (compared to the SD assumption) where the

inter-grain interaction plays an important role. We also analyze the sample-to-sample variations and stochastic  $P$ -switching characteristics and investigate its correlation with FE thickness scaling.

## II. 3D MODELING FRAMEWORK

Our modeling framework for polycrystalline HZO consists of 3D grain growth simulation coupled with 3D phase-field simulation. In the grain growth simulation, a polycrystalline microstructure is represented by multiple dimensionless order parameters ( $\eta_k$ ) whose temporal and spatial evolution follows a time-dependent Ginzburg-Landau [9] type equation (shown in Fig. 2). Then each order parameter ( $\eta$ ) is mapped across a range of crystallization angles ( $\theta$ ). Here, we define the crystal coordinate as  $(a, b, c)$  and global coordinate as  $(x, y, z)$  where the  $z$ -axis represents the physical thickness direction of the FE film. The  $P$  direction in the orthorhombic crystal phase is parallel to the  $c$ -axis. The crystallization angle,  $\theta$  defines the angle between the  $z$ -axis and  $c$ -axis. In the phase-field model, we solve the TDGL equation with  $P$  as the state variable considering the crystal coordinate system self-consistently with Poisson's equation considering the global coordinate system. The complete simulation flow and the simulation parameters are shown in Fig. 2. All the equations are solved in real space by following the finite-difference approach.

## III. CALIBRATION OF 3D GRAIN-GROWTH AND PHASE-FIELD MODEL

In our simulation, we consider a MFIM with HZO ( $\text{Hf}_{0.5}\text{Zr}_{0.5}\text{O}_2$ ) as the FE and the  $\text{Al}_2\text{O}_3$  as the underlying DE layer (Fig. 3(a)). First, to validate our grain-growth model we show the time-dependent evolution of grain geometries (Fig. 3(b)). Our results signify the possibilities of grain boundaries (GBs) along the thickness for higher  $T_{FE}$ , but an absence such GBs for lower  $T_{FE}$  (Fig. 4(a)). Then, we analyze the grain size distributions for different  $T_{FE}$  (Fig. 4(b)), for which our simulation shows good agreement with the experimental results [3]. Next, to validate the phase-field simulation, we fabricate and measure the  $Q$ - $V$  characteristics of the MFIM ( $\text{HZO-Al}_2\text{O}_3$ ) stack. Our simulation results (Fig. 5(a-b)) signify good agreements with the measured  $Q$ - $V$  characteristics for different  $T_{FE}$  (5 and 7 nm) as well.

## IV. EFFECTS OF CRYSTAL ANGLE

To evaluate the effect of crystal angle ( $\theta$ ), first, we perform the phase-field simulation of a single-grain. The simulated  $Q$ - $V$  characteristics for different  $\theta$  values (Fig. 6(a)) show a slight decrease in remanent polarization ( $P_R$ ) and coercive voltage ( $V_C$ ) with the increase in  $\theta$ . To understand this, first, let us analyze the multi-domain (MD)  $P$ -switching mechanism in the

FE layer. Formation of MD state occurs to suppress the depolarization electric ( $E$ )-field in FE by forming in-plane  $E$ -field (stray field) in the FE interface [6-7]. This leads to non-homogeneous electric-field distribution in the FE layer. In addition to the electrostatic energy associated with the stray field, there are gradient energies associated with the  $P$  variation near the domain wall DW ( $\sim(dP/dx)^2$  and  $\sim(dP/dy)^2$ ) and the FE interface ( $\sim(dP/dz)^2$ ). Therefore, the applied voltage ( $V_{APP}$ )-induced depolarization electric-field and the gradient energy components lead to MD  $P$ -switching in the FE layer due to the non-homogeneity in the local energy density. The  $P$ -switching initiates with DW displacement, followed by domain nucleation and then again DW motion. With the increase in  $\theta$ ,  $P_R$  decreases and  $V_C$  shows slight reduction (**Fig. 6(b-c)**) because of the increase in effective gradient energy coefficient. Therefore, for higher  $\theta$ , we observe the formation of less number of domains during the  $P$ -switching (**Fig. 6(d-e)**). Most importantly, the effect of  $\theta$  on  $V_C$  and  $P_R$  is not significant in case of MD  $P$ -switching compared to the single-domain  $P$ -switching (**Fig. 6(b-c)**).

Now, let us analyze the correlation between the  $P$ -switching in neighboring grains. For this, we consider a two-grain scenario with one grain having  $\theta=0$  and the other with  $\theta>0$  (**Fig. 7(a)** inset). As  $V_C$  of an individual grain decreases with the increase in  $\theta$ , therefore, the  $P$ -switching initiates in the grain with  $\theta > 0$ . The  $P$ -switching in the neighboring grain leads to the local compensation of depolarization  $E$ -field in the grain with  $\theta=0$  (due to long-range Coulomb interaction) yielding a delayed  $P$ -switching. Therefore, the effective  $V_C$  of a grain can increase due to the presence of a grain with higher  $\theta$  (**Fig. 7(a)**). Further, depending on the relative difference in  $\theta$ , such inter-grain interactions (electrostatic and elastic) can lead to  $P$ -switching via DW displacement near the grain boundary (**Fig. 7(c)**,  $\theta_1=0$ ,  $\theta_2=40$ ) and/or domain nucleation (**Fig. 7(b)**,  $\theta_1=0$ ,  $\theta_2=20$ ). This analysis signifies the importance of inter-grain coupling (especially via electrostatics) in the polycrystalline FE and weaken the assumptions of complete decoupling of grains in the different  $P$ -switching models (i.e., KAI, NLS etc.) for small area FE samples.

## V. POLARIZATION SWITCHING IN POLYCRYSTALLINE FERROELECTRIC

Now, let us analyze the  $P$ -switching characteristics in polycrystalline HZO with a sample size  $20\text{nm} \times 20\text{nm} \times 5\text{nm}$  that exhibits multiple grains with different  $\theta$ . The simulated  $Q$ - $V_{APP}$  characteristics (**Fig. 8(a)**) show the evolution of minor loops with the decrease in  $\max(V_{APP})$ . More importantly, our results signify that unlike the assumptions of the previous models [4-5], the evolution of minor loops may not necessarily imply a complete  $P$ -switching in some grains and no  $P$ -switching in the rest. Rather, the minor loops can evolve with the partial or MD  $P$ -switching across all the FE grains (**Fig. 8(b)**).

Next, we analyze the cycle-cycle variation in the  $Q$ - $V_{APP}$  characteristics (**Fig. 9**). Different MD configurations corresponding to different  $P_R$  at different voltage cycles (shown in **Fig. 9(c)**) signify that the MD pattern is not unique to a

certain voltage. Rather, in each cycle, the FE layer generates different MD patterns which leads to stochastic  $P$ -switching. *It is important to note that this stochasticity is solely driven by the electrostatic and elastic interactions rather than the non-homogeneity in the parameter or the thermal fluctuations in the FE layer.* The distribution of  $P_R$  and  $V_C$  due to the cycle-to-cycle variation is shown in **Fig. 9**. Further, different FE samples yield grains with different size/shape and  $\theta$  and that can lead to a significant device-to-device variation in the  $P$ -switching characteristics in the FE layer. To investigate that, we consider 250 different samples with different grain profiles and the corresponding distribution in the  $P_R$  and  $V_C$  is shown in **Fig. 10**.

## VI. EFFECTS OF FERROELECTRIC THICKNESS ON SAMPLE-TO-SAMPLE VARIATION AND CYCLE-TO-CYCLE STOCHASTICITY

As the MD switching leads to sample-to-sample variations (compared to the SD scenario) and causes stochastic  $P$ -switching therefore, it is important to analyze these properties in the context of FE thickness ( $T_{FE}$ ) scaling due to its correlation with the domain density [8] (**Fig. 9-10**). The domain pattern for different  $T_{FE}$  signify the evolution of denser domain pattern and a transition from nucleation dominant to DW motion dominant  $P$ -switching in the FE layer with the reduction in  $T_{FE}$ . It is important to note that, both the variation and stochasticity is more dominant in the case of nucleation-driven switching (due to the random shape and size of the nucleated domains) compared to the DW motion-driven switching (only the relative size of the domains changes). Therefore, we observe a lower sample-to-sample variation and lower stochasticity with the reduction in  $T_{FE}$  (**Fig. 9-10**).

## VII. CONCLUSION

In summary, we developed a 3D grain-growth coupled phase field model for HZO-based MFIM and analyzed the multi-domain (MD) polarization ( $P$ ) switching characteristics in polycrystalline FE HZO. Our analysis signifies that variation in  $V_C$  and  $P_R$  due to polycrystallinity can be suppressed because of the MD  $P$ -switching where the electrostatic and elastic coupling among the grains play an important role. Further, we analyzed the sample-to-sample variations and cycle-to-cycle stochasticity in the  $P$ -switching dynamics and show that FE thickness scaling can suppress both variation and stochasticity in low area FE-based devices.

## ACKNOWLEDGMENT

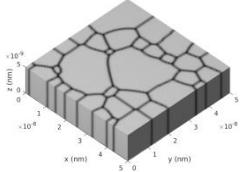
This work was supported by SRC (2020-LM-2959) and NSF (2008412).

## REFERENCES

- [1] K. Chatterjee, et al., *IEEE Elect. Dev. Lett.*, vol. 38, no. 10, 2017.
- [2] M. Jerry et al., *IEDM*, 6.2.1-6.2.4, 2017.
- [3] M. H. Park et al., *Nanoscale*, vol. 9, no. 28, 2017.
- [4] M. Materano et al., *Appl. Phys. Lett.*, vol. 117, no. 26, 2020.
- [5] C Garg, et al., *IEEE Electron Dev. Lett.*, vol. 42, no. 8, 2021.
- [6] A. K. Saha et al., *Scientific Reports*, vol. 10, no. 1, 2020.
- [7] A. K. Saha et al., *J. Appl. Phys.*, vol. 129, no. 8, 2021.
- [8] A. K. Saha et al., *IEDM*, 4.3.1-4.3.4, 2020.
- [9] C. E. Krill III et al., *Acta Materialia*, vol. 50, 2002.

### 3D Phase-field Simulation coupled with Grain Growth Model

#### Polycrystalline HZO



#### 3D Grain Growth Equation

$$\frac{\partial \eta_k(\mathbf{r}, t)}{\partial t} = -L(-\alpha \eta_k(\mathbf{r}, t) + \beta \eta_k^3(\mathbf{r}, t) + 2\gamma \eta_k(\mathbf{r}, t) \sum_{s \neq k}^K \eta_s^2(\mathbf{r}, t) - \kappa \nabla^2 \eta_k(\mathbf{r}, t))$$

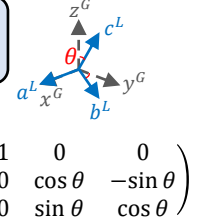
#### 3D Poisson's Equation

$$-\epsilon_0 \left[ \frac{\partial}{\partial x} \left( \epsilon_x \frac{\partial \phi}{\partial x} \right) + \frac{\partial}{\partial y} \left( \epsilon_y \frac{\partial \phi}{\partial y} \right) + \frac{\partial}{\partial z} \left( \epsilon_z \frac{\partial \phi}{\partial z} \right) \right] = -\frac{dP_x^G}{dx} - \frac{dP_y^G}{dy} - \frac{dP_z^G}{dz}$$

#### Time-Dependent Ginzburg Landau (TDGL)

$$-\frac{1}{\Gamma} \frac{\partial P_c^L}{\partial t} = \alpha P_c^L + \beta (P_c^L)^3 + \gamma (P_c^L)^5 - g_{11} \frac{dP_c^L}{da^2} - g_{22} \frac{dP_c^L}{db^2} - g_{33} \frac{dP_c^L}{dc^2} + \frac{d\phi}{dc}$$

$$\lambda \frac{dP_c^L}{dc} - P_c = 0$$



$$\begin{bmatrix} P_a^L \\ P_b^L \\ P_c^L \end{bmatrix} = R \begin{bmatrix} P_x^G \\ P_y^G \\ P_z^G \end{bmatrix}$$

$$\alpha = -2.3 \times 10^9 \text{Vm/C}; \quad g_{11} = 7 \times 10^{-11} \text{Vm}^3/\text{C}; \quad \epsilon_{FE} = 23;$$

$$\beta = -4.5 \times 10^9 \text{Vm}^5/\text{C}^3; \quad g_{22} = 7 \times 10^{-11} \text{Vm}^3/\text{C}; \quad \epsilon_{DE} = 10;$$

$$\gamma = 1.7 \times 10^{11} \text{Vm}^9/\text{C}; \quad g_{33} = 2 \times 10^{-11} \text{Vm}^3/\text{C}; \quad \lambda = 3\text{nm};$$

#### Previous Models [4], [5]

- Assumes a distribution of remanent-P and coercive voltage in different grains.
- Independent P-switching among grains.

#### This work –

- Remanent-P and coercive voltage depends on the crystallographic angle.
- Correlated multi-domain P-switching among the grains due to electrostatic and elastic coupling
- Captures Physics driven stochasticity.

Fig. 1: Comparison of this work with previous modeling approaches.

Fig. 2: 3D Grain growth model coupled with 3D phase-field simulation (Poisson's + TDGL equations) and simulation flow; simulation parameters and transformation matrix for global and crystal coordinate.

### Model Calibration and Polycrystalline HZO grain structure

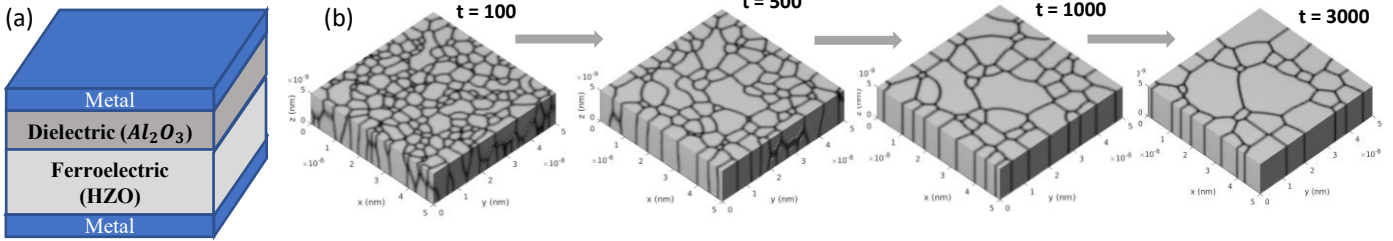


Fig. 3: (a) Metal-FE-Insulator-Metal (MFIM) structure, (b) Time ( $t$ ) evolution of polycrystalline grain structures for 5nm HZO from grain-growth simulation.

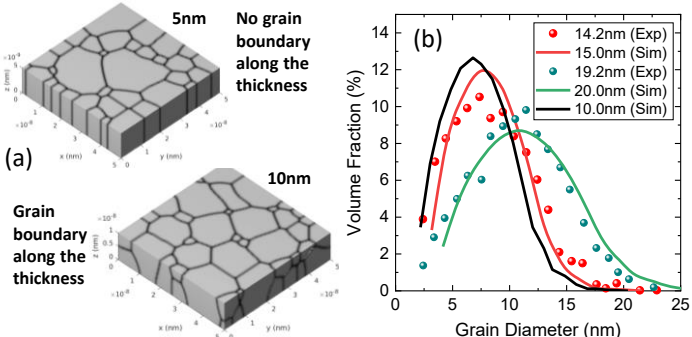


Fig. 4: (a) Grain structures for two different FE thicknesses – 5nm and 10nm, (b) Simulated and experimental [3] grain size distribution for different FE thickness ( $T_{FE}$ ).

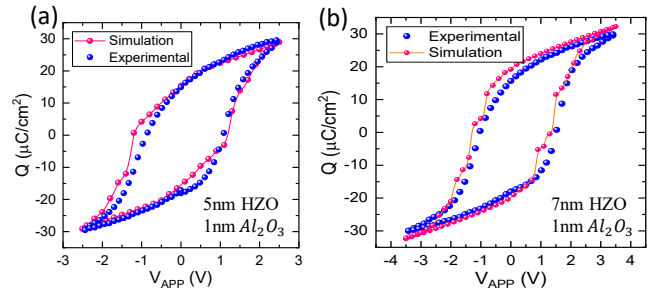


Fig. 5: Simulated and experimental charge ( $Q$ ) vs applied voltage ( $V_{APP}$ ) characteristics of MFIM stacks for two different FE thicknesses – (a) 5nm and (b) 7nm.

### Effects of crystal orientation (single grain)

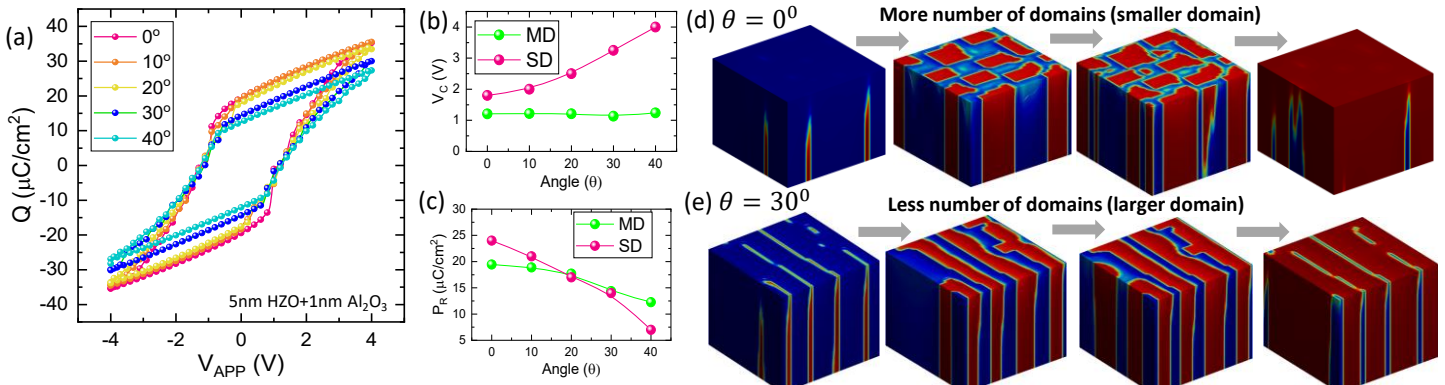
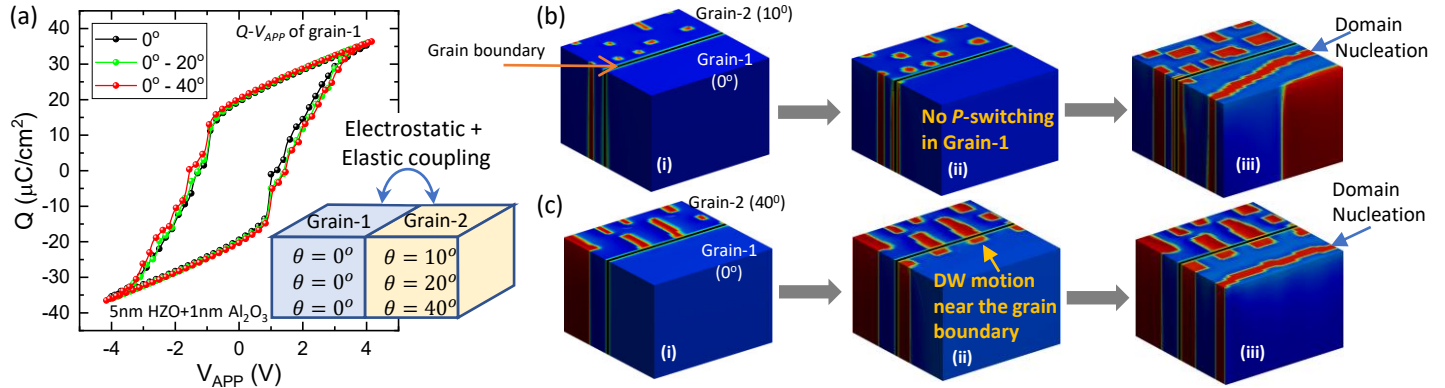


Fig. 6: (a)  $Q$ - $V_{APP}$  characteristics of MFIM stack (5nm HZO+1nm  $\text{Al}_2\text{O}_3$ ) considering single grain with different crystallization angle ( $\theta$ ). (b) Remanent Polarization ( $P_R$ ) and (c) coercive voltage ( $V_C$ ) for different  $\theta$  signifying less variation in  $P_R$  and  $V_C$  for MD  $P$ -switching compared to single-domain L-K based  $P$ -switching. (d)-(e) Multi-domain  $P$ -switching for  $\theta = 0^\circ$  and  $30^\circ$  signifying a smaller number of domains for higher  $\theta$  due to increase in effective gradient energy coefficient with increasing  $\theta$ .

### Effects of $P$ -switching in Neighboring Grain with different $\theta$ (Electrostatic and Elastic Interaction)



**Fig. 7:** (a)  $Q$  vs  $V_{APP}$  loops showing the effect of Grain-2 orientation on Grain-1 of  $0^\circ$  compared to single grain scenario, (b) Multi domain  $P$ -switching for Grain-1  $\theta = 0^\circ$  and Grain-2  $\theta = 10^\circ$  and (c) for Grain-1  $\theta = 0^\circ$  and Grain-2  $\theta = 40^\circ$  showing the domain wall motion (or domain growth) near grain boundary.

### Effects of polycrystallinity

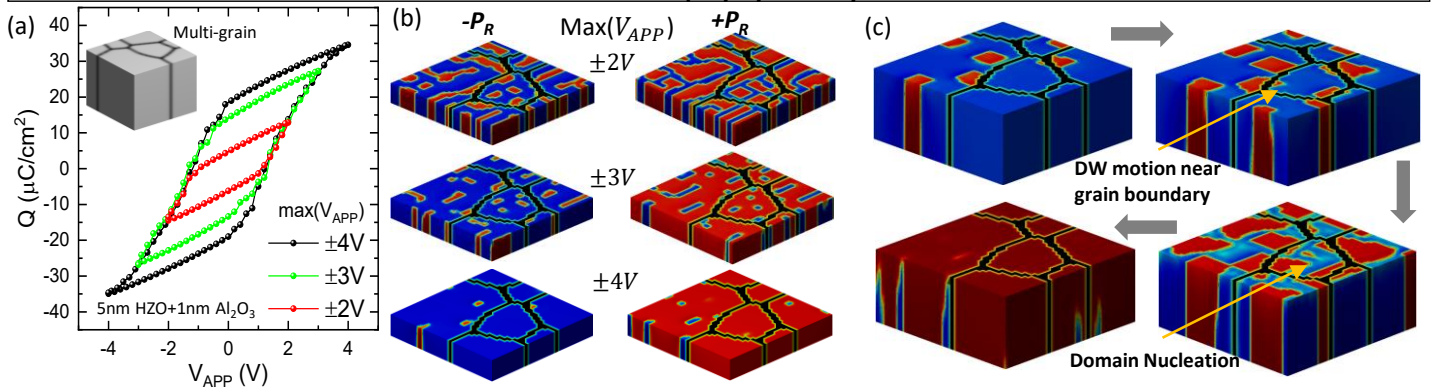


**Fig. 8:** (a) Grain structure of simulated  $20\text{nm} \times 20\text{nm} \times 5\text{nm}$  HZO (inset) and  $Q$  vs  $V_{APP}$  of MFIM stack for different  $\max(V_{APP})$ , (b) Domain structures at  $V_{APP} = 0\text{V}$  (representing  $P_R$ ) for different maximum  $V_{APP}$ . (c) Multi domain configurations signifying the effect of adjacent grains on the polarization switching mechanism.

### FE Thickness dependence of stochasticity and variations

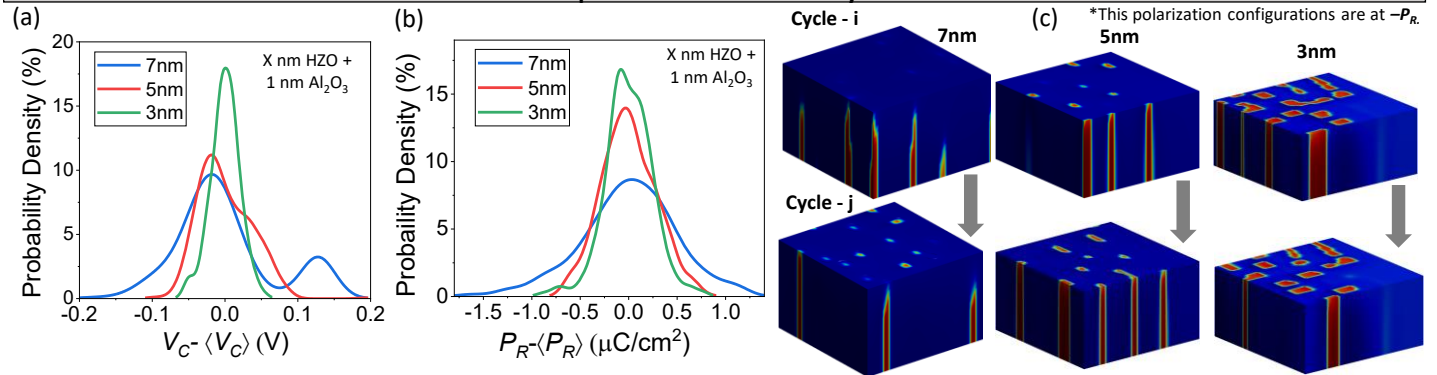


**Fig. 9:** Cycle-to-cycle variation (stochasticity) of (a) coercive voltage ( $V_C$ ) and, (b) remnant polarization ( $P_R$ ) with different FE thickness. (c) Domain structures showing the different domain patterns at 0V during different cycles giving rise to cycle-to-cycle variation in  $P_R$ .  $\langle V_C \rangle$  and  $\langle P_R \rangle$  represent mean value.

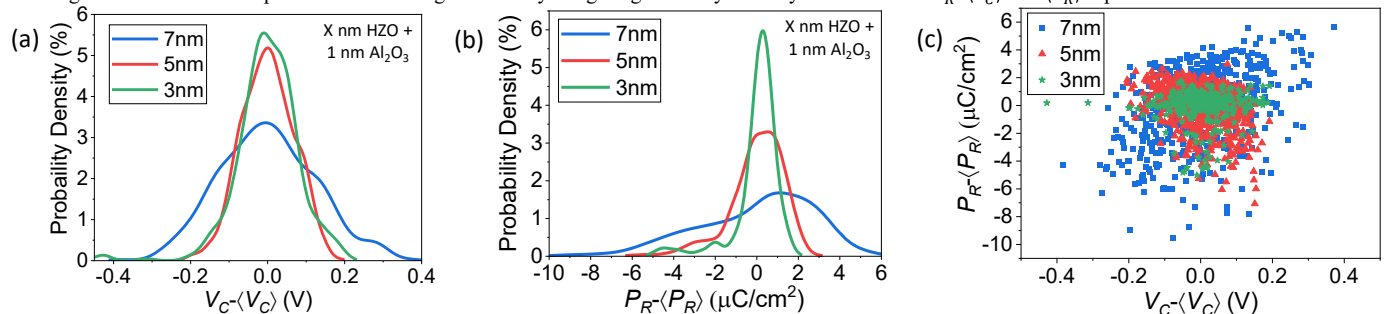


**Fig. 10:** Sample-to-sample variation of (a) coercive voltage ( $V_C$ ) and, (b) remnant polarization ( $P_R$ ) with different FE thickness signifying that the variation reduces with the decrease in FE thickness. (c) Scatter plot showing the correlation of sample-to-sample variation with the FE thickness.  $\langle V_C \rangle$  and  $\langle P_R \rangle$  represent mean value.